Geometric Cue for Protein Localization in a Bacterium

Kumaran S. Ramamurthi, *et al.*

Science **323**, 1354 (2009);
DOI: 10.1126/science.1169218

Geometric Cue for Protein Localization in a Bacterium

Kumaran S. Ramamurthi,[1] Sigolene Lecuyer,[2] Howard A. Stone,[2] Richard Losick[1]*

Proteins in bacteria often deploy to particular places within the cell, but the cues for localization are frequently mysterious. We found that the peripheral membrane protein SpoVM (VM) recognizes a geometric cue when localizing to a particular membrane during sporulation in *Bacillus subtilis*. Sporulation involves an inner cell maturing into a spore and an outer cell nurturing the developing spore. VM is produced in the outer cell, where it embeds in the membrane that surrounds the inner cell but not in the cytoplasmic membrane of the outer cell. We found that VM localized by discriminating between the positive curvature of the membrane surrounding the inner cell and the negative curvature of the cytoplasmic membrane. Membrane curvature could be a general cue for protein localization in bacteria.

Proteins often localize to particular positions within bacteria, sometimes in a dynamic manner. A striking but mysterious example of subcellular localization occurs during spore formation in *Bacillus subtilis* when the protein SpoVM (VM) localizes to a particular patch of membrane (*1*). How VM discriminates between different membrane surfaces in the same cell is unknown.

During sporulation, the cell divides asymmetrically to create mother-cell and forespore compartments. Next, the mother cell engulfs the forespore, enveloping it with inner and outer membranes (Fig. 1A). After engulfment, a protein coat is deposited around the outer forespore membrane (*2*). Coat assembly depends on VM, a 26-residue peptide that is produced in the mother cell (*3*). VM is an amphipathic α helix (*4*) that inserts into the membrane with its long axis parallel to the membrane and its hydrophobic face buried in the lipid bilayer (*5*). During engulfment, VM localizes to the membrane that tracks around the forespore, eventually decorating the entire surface of the forespore, as visualized by its fusion to green fluorescent protein (VM-GFP) (Fig. 1C) (*1*). Proline 9 (P9) (Fig. 1B) is critical for this localization (*1*), because substitution of P9 with alanine (VM^{P9A}-GFP) resulted in localization to both the cytoplasmic and outer forespore membranes (Fig. 1D).

After engulfment, the outer forespore membrane becomes topologically isolated from the cytoplasmic membrane. We wondered if VM would adhere to the outer forespore membrane after isolation. We engineered cells to produce VM-GFP in response to an inducer and triggered synthesis of the fusion protein after engulfment. To monitor topological isolation, we stained the membranes with a membrane-permeating dye, which stains all membranes, and a nonpermeating dye, which can only access the engulfment membrane before membrane fusion (*6*). VM-GFP was localized almost exclusively to the outer forespore membrane even when the forespore was topologically isolated (Fig. 1, G to I). As a control, VM^{P9A}-GFP synthesized after engulfment localized promiscuously (Fig. 1, J to L). Thus, VM-GFP partitions between both membranes, but the wild-type fusion protein is retained in the outer forespore membrane.

What does VM recognize? We wondered whether the localization cue for VM was geometric, because the outer forespore membrane is the only membrane in the mother cell with a positive (convex) curvature. We examined the localization of VM-GFP in cells of a triple mutant [SpoIID/SpoIIM/SpoIIP (D/M/P)] arrested with a straight polar septum (*7*). VM-GFP behaved indiscriminately in such mutant cells, localizing to the cytoplasmic and engulfing membranes (Fig. 2B).

As a further test of the idea that VM recognizes curvature, we took advantage of the fact that at low frequency (~1%) the D/M/P triple mutant develops a fissure in the septum, allowing the membrane to bulge into the mother cell (*8*). VM-GFP should localize to this convex membrane protrusion. Indeed, VM-GFP localized with high selectivity to such bulges (Fig. 2C).

[1]Department of Molecular and Cellular Biology, Harvard University, Cambridge, MA 02138, USA. [2]School of Engineering and Applied Sciences, Harvard University, Cambridge, MA 02138, USA.

*To whom correspondence should be addressed. E-mail: losick@mcb.harvard.edu

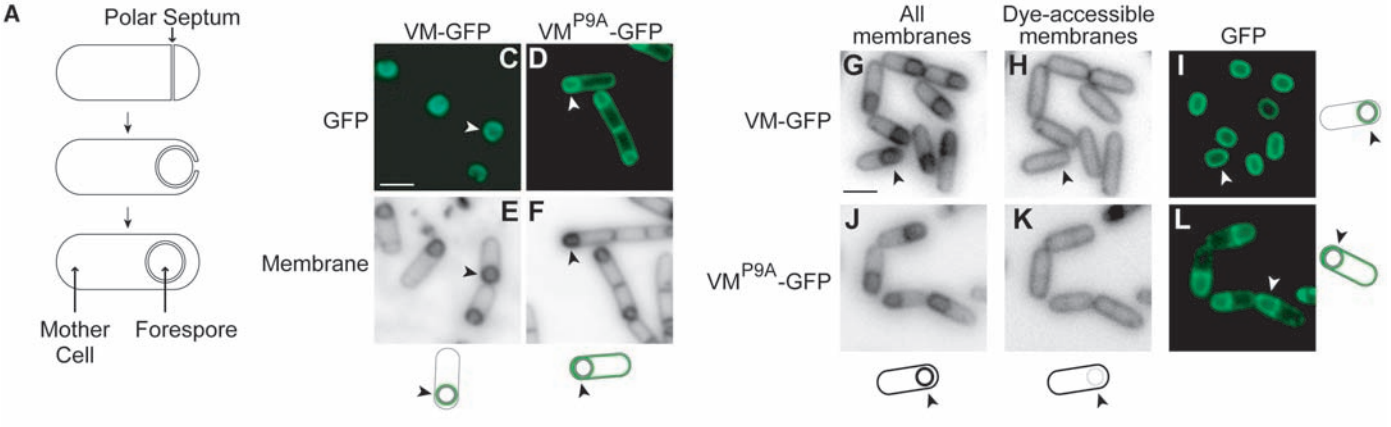

Fig. 1. VM-GFP localizes selectively to the surface of the forespore (*11*). (**A**) Stages of sporulation. (Top) Division creates a mother cell (left) and a forespore (right). (Middle) The mother cell engulfs the forespore. (Bottom) The forespore is pinched off as a protoplast. (**B**) α-helical model of VM. Shown on the left is the hydrophobic membrane-embedded face and on the right a 180° rotation of the helix along its long axis with positively charged residues labeled green. A, alanine; F, phenylalanine; I, isoleucine; K, lysine; L, leucine; M, methionine; P, proline; R, arginine; T, threonine; V, valine; Y tyronine. N refers to the amino terminus. Red square indicates proline 9; gray circles indicate hydrophobic residues on the positively charged face. (**C**) VM-GFP localizes to the surface of the forespore, whereas VM^{P9A}-GFP localizes to all membranes (**D**). (**E** and **F**) Membrane-stained cells in (C) and (D), respectively. Arrowheads identify the cell depicted in the illustrations. (**G** to **L**) Localization of VM-GFP or VM^{P9A}-GFP produced after topological isolation. The membrane surrounding the forespore was stained by a membrane-permeating dye [(G) and (J)] but not by a nonpermeating dye [(H) and (K)]. VM-GFP (I), but not VM^{P9A}-GFP (L), localized selectively to the surface of the forespore. Scale bars, 2 μm.

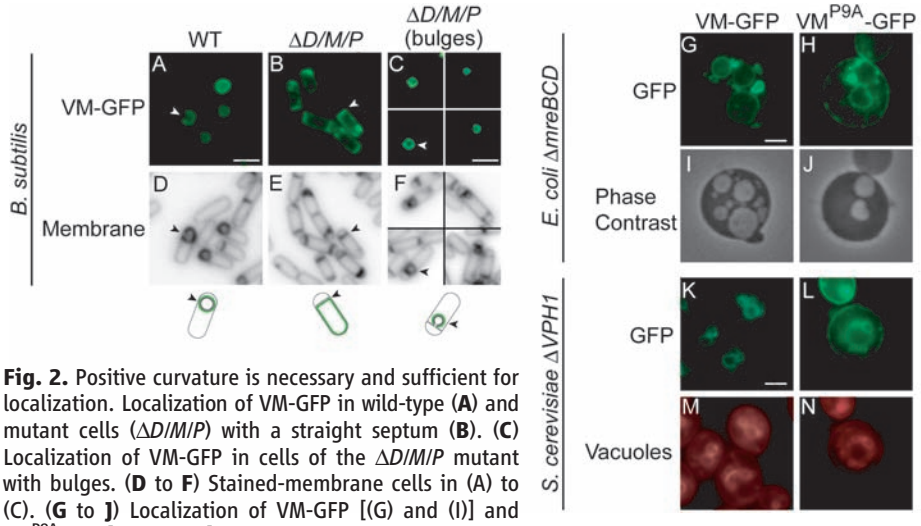

Fig. 2. Positive curvature is necessary and sufficient for localization. Localization of VM-GFP in wild-type (**A**) and mutant cells (Δ*D/M/P*) with a straight septum (**B**). (**C**) Localization of VM-GFP in cells of the Δ*D/M/P* mutant with bulges. (**D** to **F**) Stained-membrane cells in (A) to (C). (**G** to **J**) Localization of VM-GFP [(G) and (I)] and VM^{P9A}-GFP [(H) and (J)] in mutant *E. coli* cells (Δ*mreBCD*) that produce internal vesicles. [(I) and (J)] Vesicles were visualized by phase contrast microscopy. (**K** to **N**) Localization of VM-GFP [(K) and (M)] and VM^{P9A}-GFP [(L) and (N)] in mutant yeast cells (Δ*VPH1*) that produced fragmented vacuoles. [(I) and (J)] Vacuoles were stained with FM4-64. Scale bars, 2 μm.

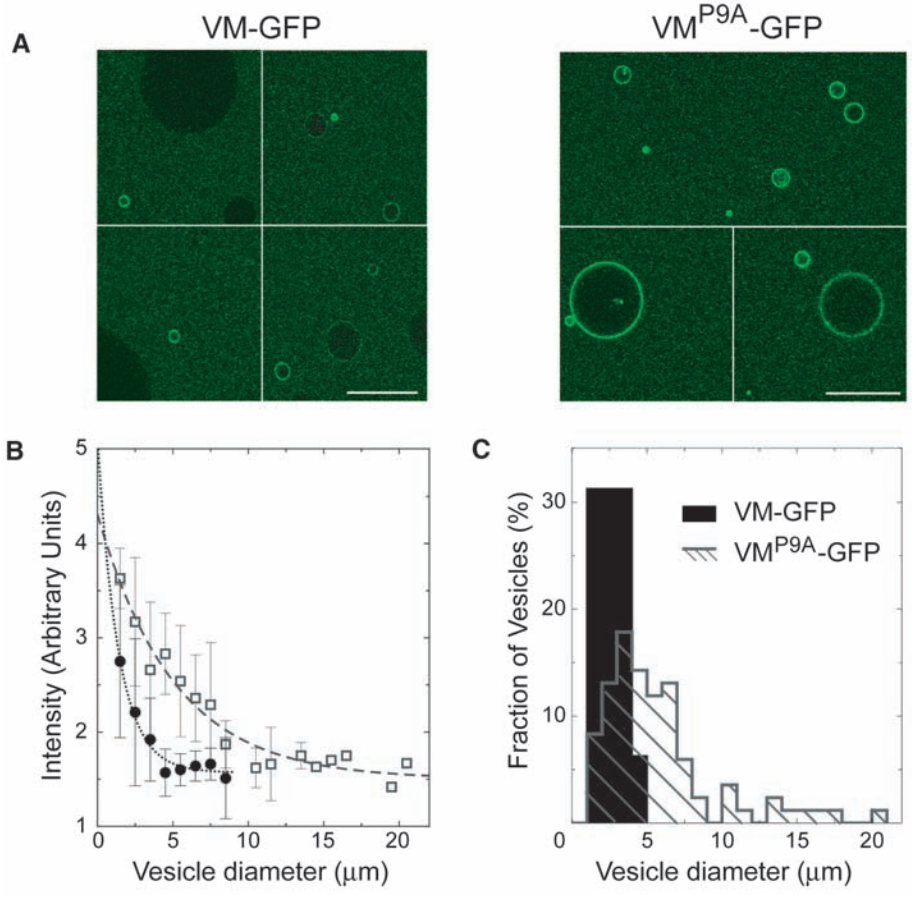

Fig. 3. VM-GFP detects curvature in vitro. (**A**) Confocal fluorescence micrographs of purified VM-GFP (left) or VM^{P9A}-GFP (right) incubated with phospholipid vesicles. Scale bars, 20 μm. (**B**) Membrane fluorescence intensity as a function of vesicle diameter. Vesicles were incubated with similar concentrations of VM-GFP (solid circles) or VM^{P9A}-GFP (open squares). The data points are mean ± SD measured on *n* vesicles (*n* = 3 to 18) and were fit with an exponential decay (*11*). (**C**) Size distribution of fluorescent vesicles whose intensity is at least 2.5-fold greater than the background.

To test the curvature hypothesis, we examined the localization of VM-GFP in a heterologous host that also exhibits convex membranes, an *Escherichia coli* mutant lacking the cytoskeletal protein MreB (*9*) that forms internal vesicles similar in size to the forespore. In mutant cells, VM-GFP localized almost exclusively to the surface of the vesicles (Fig. 2G). As a control, VM^{P9A}-GFP not only localized to the surface of vesicles but also to the cytoplasmic membrane (Fig. 2H). We also examined the localization of VM-GFP in a mutant of *Saccharomyces cerevisiae* that produces fragmented vacuoles whose sizes are again similar to that of the forespore (*10*). In these cells, VM-GFP localized primarily to the surface of vacuoles, whereas VM^{P9A}-GFP localized to the concave periphery of the cells as well (Fig. 2, K and L). VM-GFP and VM^{P9A}-GFP were stable and was produced at similar levels in *B. subtilis*, *E. coli*, or *S. cerevisiae* (fig. S1). Taken together, VM appears to respond to a geometric cue rather than a *B. subtilis*–specific feature of the membrane.

If so, then VM should bind preferentially to any phospholipid bilayer with a curvature similar to that of the outer forespore membrane. We asked whether purified VM-GFP would adsorb to the surface of phosphoplipid vesicles and whether it would favor vesicles similar in size to the forespore. We prepared by means of electroformation a heterogeneously sized population of unilamellar phospholipid vesicles, ranging in diameter from approximately 1 to 30 μm, with a distribution that peaked at 8 μm (*11*). We incubated the vesicles with purified VM-GFP harboring a C-terminal polyhistidine tag (VM-GFP-His$_6$) and examined the distribution of fluorescence with confocal laser microscopy. VM-GFP preferentially adsorbed to the smallest observable vesicles in the population (Fig. 3A). In contrast, VM^{P9A}-GFP displayed a diminished preference for smaller vesicles and adsorbed to the surfaces of even large vesicles (Fig. 3A). The fluorescent signal resulted from surface-localized VM-GFP-His$_6$, and a label introduced into the lipids resulted in uniform and equally fluorescent vesicles (*11*).

The concentration of surface-adsorbed VM-GFP decreased as the diameter of the vesicles increased (Fig. 3B). Thus, smaller vesicles harbored more VM-GFP per surface area than did larger vesicles. When vesicles were incubated with VM^{P9A}-GFP, however, the decrease of fluorescence intensity with increasing vesicle size was much less pronounced, suggesting that VM^{P9A}-GFP was recruited more readily to larger vesicles (Fig. 3B). Next, we measured the number of vesicles whose fluorescence was at least 2.5 times higher than background fluorescence (Fig. 3C). Strong adsorption of VM-GFP occurred for vesicles less than 5 μm in diameter and peaked near the smallest vesicles in the population at around 2.5 μm in diameter (by comparison, a forespore is approximately 1 μm in diameter). In our analysis, vesicles less than 1 μm in diameter were grossly

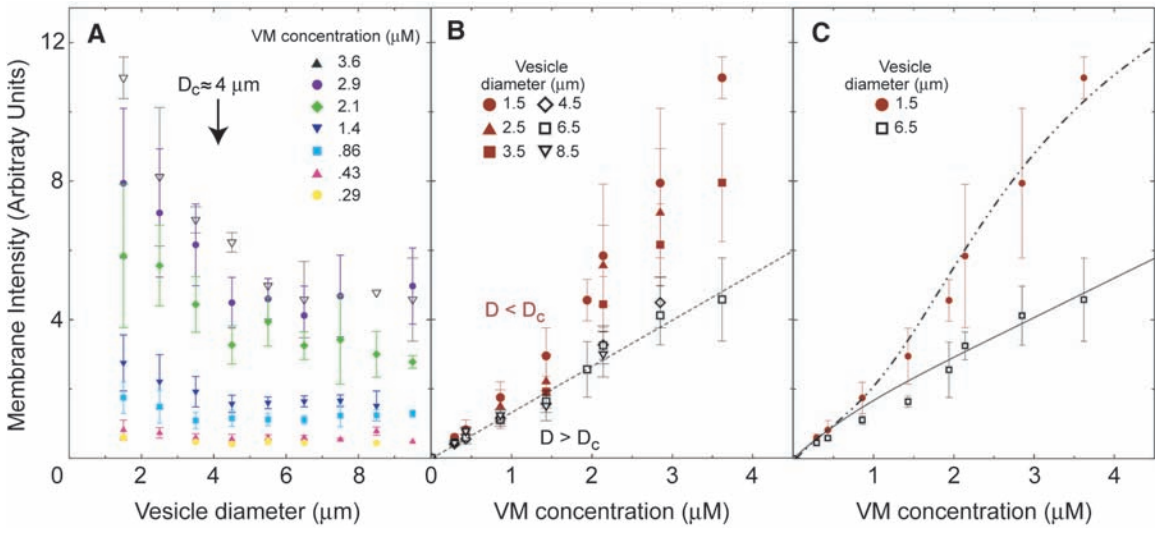

Fig. 4. Preferential adsorption of VM-GFP onto smaller vesicles is concentration-dependent. (**A**) Membrane fluorescence intensity as a function of vesicle diameter for increasing bulk concentrations of VM-GFP. At higher concentrations, vesicles with a diameter below D_c ~ 4 μm were preferentially labeled. (**B**) Membrane fluorescence intensity as a function of VM-GFP concentration for different vesicle diameters (indicated diameters are ±0.5 μm). Above D_c, all data points were similar and well approximated by a linear fit (dotted line), whereas below D_c the isotherms were steeper and deviated from linear. (**C**) Typical behaviors for small (1.5 ± 0.5 μm) and large (6.5 ± 0.5 μm) vesicles and theoretical curves obtained using a model for cooperativity (*11*). Data points are mean ± SD measured on *n* vesicles (*n* = 3 to 26), resulting from three independent experiments.

underrepresented. Thus, we probably overestimated the peak size of vesicles to which VM-GFP was recruited, and VM-GFP may preferentially adsorb onto even smaller vesicles (Figs. 3B and 4A). In contrast to VM-GFP, VM^{P9A}-GFP adsorbed onto vesicles up to 20 μm in diameter, resulting in a broad distribution with a peak at about 5 μm. Substitution of P9 does not simply increase the affinity of VM for membranes. Thus, the adsorption of VM-GFP to membranes is sensitive to curvature and dependent on P9.

How can VM, which is 40 Å in length or less (*12*), be sensitive to the curvature of micrometer-sized spheres? A precedent is adenosine 5′-diphosphate–ribosylation factor guanosine triphosphatase–activating protein 1 (ArfGAP1), a Golgi-associated protein that preferentially associates with yeast vesicles via a stretch of α-helix (*13*, *14*) and is sensitive to curvature. But the vesicles recognized by ArfGAP1 are far smaller (~50 nm) and more highly curved than those recognized by VM. For a 40 Å rod lying flat on the surface of a 1-μm-diameter sphere, the maximum distance between one end of the rod and the surface of the sphere is less than 0.2 Å. It therefore seems improbable that the partitioning of individual VM molecules between differently sized spheres could be influenced by such a small degree of curvature. Several molecules of VM may thus be required to display a collective sensitivity for slightly curved surfaces. We tested whether the preferential adsorption of VM-GFP to smaller vesicles was dependent on the concentration of VM-GFP by measuring membrane fluorescence intensity as a function of vesicle size for different concentrations of VM-GFP. The preferential adsorption of VM-GFP onto smaller vesicles increased with increasing concentrations of protein (Fig. 4A). Moreover, our data suggest a critical value of the vesicle diameter (D_c) of about 4 μm. For all concentrations, above D_c the amount of VM-GFP adsorbed per unit area of membrane did not substantially vary. However, below D_c and at higher concentrations, the adsorbed amount strongly increased with a decreasing vesicle diameter.

We then constructed an "adsorption isotherm," which is a signature of the adsorption mechanism. For a given vesicle diameter, we plotted membrane fluorescence intensity as a function of VM-GFP bulk concentration (Fig. 4B). When the vesicle diameter was larger than D_c, all curves were similar and approximately linear, indicating that the adsorption mechanism was the same and not dependent on membrane curvature. However, below D_c the curves deviated from linear and became progressively steeper as the vesicle diameter decreased, which suggests an adsorption mechanism that involves cooperative interactions (clustering) among VM-GFP. Preliminary theoretical analysis points to clusters consisting of just a few VM molecules (fig. S2) (*11*). VM-GFP molecules do not appear to interact with each other directly (fig. S3). An alternative possibility, however, and one that we favor, is that the insertion of a VM molecule into the membrane indirectly recruits other VM molecules to its vicinity analogous to the clustering of certain phospholipids (*15*) and membrane proteins (*16*, *17*): The energetic cost due to bilayer deformation induced by the insertion of VM could be minimized by the clustering of VM molecules, resulting in an apparent cooperativity that does not involve contact between protein molecules.

Might geometric cues represent a strategy by which proteins localize to particular patches of membrane in bacteria? Convex surfaces, such as that of the forespore, are not typical in bacteria. Nonetheless, some bacteria produce organelles with positively curved membranes, such as photosynthetic vesicles and magnetosomes (*18*, *19*). Perhaps amphipathic α-helices are used to identify the membranes of these organelles for protein localization. A major challenge in bacterial cell biology is to identify cues that recruit proteins to the poles of cells. Conceivably, membrane curvature, in this case extreme negative curvature, is used to identify the inside surface at the pole.

References and Notes

1. C. van Ooij, R. Losick, *J. Bacteriol.* **185**, 1391 (2003).
2. A. O. Henriques, C. P. Moran Jr., *Annu. Rev. Microbiol.* **61**, 555 (2007).
3. P. A. Levin *et al.*, *Mol. Microbiol.* **9**, 761 (1993).
4. R. S. Prajapati, T. Ogura, S. M. Cutting, *Biochim. Biophys. Acta* **1475**, 353 (2000).
5. K. S. Ramamurthi, K. R. Clapham, R. Losick, *Mol. Microbiol.* **62**, 1547 (2006).
6. D. Z. Rudner, Q. Pan, R. M. Losick, *Proc. Natl. Acad. Sci. U.S.A.* **99**, 8701 (2002).
7. P. Eichenberger, P. Fawcett, R. Losick, *Mol. Microbiol.* **42**, 1147 (2001).
8. B. Blaylock, X. Jiang, A. Rubio, C. P. Moran Jr., K. Pogliano, *Genes Dev.* **18**, 2916 (2004).
9. F. O. Bendezu, P. A. de Boer, *J. Bacteriol.* **190**, 1792 (2008).
10. E. S. Seeley, M. Kato, N. Margolis, W. Wickner, G. Eitzen, *Mol. Biol. Cell* **13**, 782 (2002).
11. Materials and methods are available as supporting material on *Science* Online.
12. D. J. Barlow, J. M. Thornton, *J. Mol. Biol.* **201**, 601 (1988).
13. R. Parthasarathy, J. T. Groves, *Soft Matter* **3**, 24 (2007).
14. J. Bigay, J. F. Casella, G. Drin, B. Mesmin, B. Antonny, *EMBO J.* **24**, 2244 (2005).
15. K. C. Huang, R. Mukhopadhyay, N. S. Wingreen, *PLoS Comput. Biol.* **2**, e151 (2006).
16. M. Goulian, R. Bruinsma, P. Pincus, *Europhys. Lett.* **22**, 145 (1993).
17. K. S. Kim, J. Neu, G. Oster, *Biophys. J.* **75**, 2274 (1998).

18. C. Mackenzie *et al.*, *Annu. Rev. Microbiol.* **61**, 283 (2007).
19. A. Komeili, Z. Li, D. K. Newman, G. J. Jensen, *Science* **311**, 242 (2006).
20. We thank R. Gaudet, D. Rudner, C. Schmidt, L. Shapiro, R. Schekman, D. Weitz, and N. Wingreen for discussions and S. Lacefield, B. Scheid, and P. de Boer for advice. This work was supported by the Harvard Nanoscale Science and Engineering Center, a Fulbright grant to S.L., and NIH grant GM18568 to R.L.

Supporting Online Material
www.sciencemag.org/cgi/content/full/323/5919/1354/DC1
Materials and Methods
Figs. S1 to S3
Table S1
References

2 December 2008; accepted 13 January 2009
10.1126/science.1169218

A Kinase-START Gene Confers Temperature-Dependent Resistance to Wheat Stripe Rust

Daolin Fu,[1]*† Cristobal Uauy,[1]*‡ Assaf Distelfeld,[1,2]* Ann Blechl,[3] Lynn Epstein,[4] Xianming Chen,[5] Hanan Sela,[2] Tzion Fahima,[2] Jorge Dubcovsky[1]§

Stripe rust is a devastating fungal disease that afflicts wheat in many regions of the world. New races of *Puccinia striiformis*, the pathogen responsible for this disease, have overcome most of the known race-specific resistance genes. We report the map-based cloning of the gene *Yr36* (*WKS1*), which confers resistance to a broad spectrum of stripe rust races at relatively high temperatures (25° to 35°C). This gene includes a kinase and a putative START lipid-binding domain. Five independent mutations and transgenic complementation confirmed that both domains are necessary to confer resistance. *Yr36* is present in wild wheat but is absent in modern pasta and bread wheat varieties, and therefore it can now be used to improve resistance to stripe rust in a broad set of varieties.

Bread wheat (*Triticum aestivum* L.) provides ~20% of the calories consumed by humankind. The increasing world demand for cereals requires improved strategies to reduce yield losses due to pathogens. Wheat stripe rust, caused by the fungus *Puccinia striiformis* f. sp. *tritici* (PST, table S1), affects millions of hectares of wheat, and virulent races that have appeared within the past decade are causing large yield losses (*1*–*3*). Historically, resistant varieties have provided an economical and "environmentally friendly" method to control stripe rust. Numerous race-specific resistance genes have been deployed by breeders, but each has had limited durability, presumably because of rapid pathogen evolution. In contrast, partial resistance genes (i.e., "slow-rusting") offer a broader spectrum of resistance than race-specific genes; they are generally more effective at adult plant stages and usually confer more durable resistance (*1*). Unfortunately, our understanding of partial resistance to cereal rusts is limited because none of these genes has yet been cloned.

We report here the positional cloning of the high-temperature stripe rust resistance gene *Yr36*. This gene was first discovered in wild emmer wheat (*T. turgidum* ssp. *dicoccoides* accession FA15-3, henceforth DIC) (*4*). Analysis of *Yr36* isogenic lines in different genetic backgrounds confirmed that this gene confers partial resistance to PST under field conditions and is associated with significant yield increases when the pathogen is present. In controlled environments, plants with *Yr36* are resistant at relatively high temperatures (25° to 35°C) but susceptible at lower temperatures (e.g., 15°C) (*4*). *Yr36* resistance, originally discovered in adult plants, has some effectiveness in seedlings at high temperatures (fig. S1). Other high-temperature partial resistance genes have provided durable resistance to stripe rust and are used frequently in wheat breeding programs (*5*–*8*).

To clone *Yr36*, we crossed the susceptible durum wheat variety Langdon (LDN, Fig. 1A) with the resistant isogenic recombinant substitution line RSL65 (Fig. 1B), which carries *Yr36* in a LDN genetic background. We screened a population of 4500 F_2 plants using *Yr36* flanking markers *Xucw71* and *Xbarc136* (*4*) and identified 121 lines with recombination events between these two markers. On the basis of genes from the rice colinear region (*9*), nine polymerase chain reaction (PCR) markers were developed to construct a high-density map of *Yr36* (Fig. 1, C and D, and table S2). With the use of replicated field trials and controlled environment inoculations (tables S3 and S4 and figs. S2 and S3), *Yr36* was mapped to a 0.14-cM

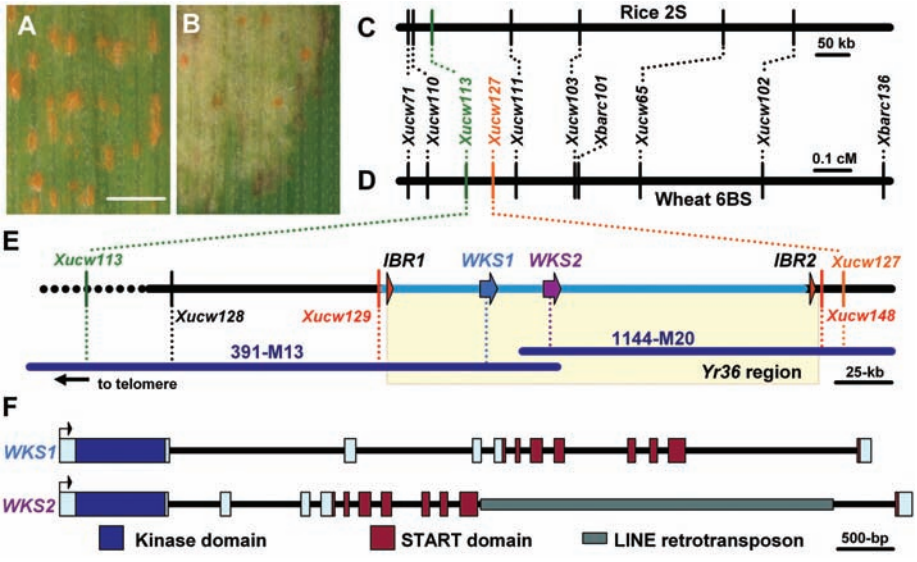

Fig. 1. Map-based cloning of *Yr36*. (**A** and **B**) Phenotype of susceptible parent Langdon with PST sporulation (A) and partially resistant parent RSL65 (B). Scale bar, 1 mm. (**C** and **D**) Genetic maps of colinear regions of rice chromosome 2 (C) and wheat chromosome 6B (D). (**E**) Physical map of the *Yr36* region. Genes are represented by colored arrows and the deleted region in Langdon by a light blue line. (**F**) Structure of the *WKS* genes. Exons are represented by rectangles, and the kinase and START domains are shown in different colors.

[1]Department of Plant Sciences, University of California, Davis, CA 95616, USA. [2]Department of Evolutionary and Environmental Biology, University of Haifa, Haifa 31905, Israel. [3]USDA-ARS, Western Regional Research Center, Albany, CA 94710, USA. [4]Department of Plant Pathology, University of California, Davis, CA 95616, USA. [5]USDA-ARS and Department of Plant Pathology, Washington State University, Pullman, WA 99164, USA.

*These authors contributed equally to this work.
†Present address: Department of Agronomy, Shandong Agricultural University, Tai'an, Shandong 271018, China.
‡Present address: John Innes Centre, Colney, Norwich NR4 7UH, UK.
§To whom correspondence should be addressed. E-mail: jdubcovsky@ucdavis.edu